

STRENGTH ANALYSIS OF A BLADE WITH DIFFERENT CROSS-SECTIONS*

Bader Somaiday¹, Ireneusz Czajka¹, Muhammad A. R. Yass²

¹AGH University of Science and Technology, Krakow, Poland

²University of Technology, Baghdad, Iraq

Abstract. *The efficiency of horizontal axis wind turbine (HAWT) blades is examined in this paper concerning the effect of cross-section airfoil type. Three different airfoils were examined: symmetric (NACA 4412), asymmetric (NACA 0012), and supercritical (NACA 4412). (EPPLER 417). The analyses that were performed combined theory and experiment. Theoretical analyses were carried out using Fortran 90 code and the blade element momentum-based Qblade code. The blade was created using SolidWorks software and a 3D printer for testing purposes. The findings of experimental tests supported the conclusions of the theory. Research revealed that the EPPLER 417 blade, which has a supercritical airfoil, performed better than other examined objects. NACA 4412, NACA 0012, and EPPLER 417 each have a power coefficient of 0.516, 0.492, and 0.510. According to the experimental data, the EPPLER 417 airfoil outperforms other airfoils in terms of power and speed reduction. To calculate the deformation and stresses of the three blades with various cross sections, CFD analysis was done in ANSYS Workbench. The CFD results showed that NACA 4412 has the highest strength but EPPLER 417 was considered the optimum cross-section based on power generation and acceptable stress values.*

Key words: HAWT, CFD analysis, Optimum power coefficient, Qblade code

1. INTRODUCTION

The aerodynamic efficiency of an airfoil is defined by the lift-to-drag ratio. It achieves the highest values at a specific angle of attack, and the value of this angle varies between airfoils. [2] The lift-to-drag ratio depends on zero-lift drag, aspect ratio, and span efficiency and is independent of weight. The use of airfoil in a wind turbine is no more limited than in an aircraft wing because a wind turbine operates at a lower speed than an aircraft. [3] There have been many theoretical and scientific studies on the performance of wind turbine blades.

Received September 29, 2022; revised December 11, 2022; accepted January 06, 2023

Corresponding author: Bader Somaiday

AGH University of Science and Technology, Krakow, Poland

E-mail: somaiday@agh.edu.pl

* An earlier version of this paper was presented at the 7th Virtual International Conference Science, Technology and Management in Energy (eEnergetics 2021), Belgrade, Serbia, December 16-17 2021 [1].

| Symbols | | | |
|----------|------------------------------|-------------|---|
| a | Axial factor | \acute{a} | Angular factor |
| C_d | Drag coefficient | C_l | Lift coefficient |
| C_p | Power Coefficient | N | Number of revolutions of rotor per minute (rpm) |
| P | Power (W) | r | Radius (m) |
| R | Radius of turbine rotor (m) | U | Wind speed (m/s) |
| α | Angle of attack (degree) | λ | Tip speed ratio |
| ϕ | Relative flow angle (degree) | Ω | Angular velocity of the rotor(rad/s) |

| Acronyms | | | |
|----------|------------------------------|-------|---|
| CFD | Computational Fluid Dynamics | HAWT | Horizontal Axis Wind Turbine |
| BEM | Blade Element Momentum | NACA | National Advisory Committee for Aeronautics |
| FEM | Finite Element Method | URANS | Unsteady Reynolds Averaged Navier-Stokes |

[4] This paper investigated an aerodynamic performance evaluation system using two groups of NACA profiles which were used in a series of five-digit NACA (63-221, 65-415; 23012,23021) and four-digit NACA (2421, 2412,4412, 4424) for three HAWT blades. The same airfoils were used along the entire blade. A computer pro-gram was developed to automate the entire procedure. Their results show that the elementary power coefficient of NACA 4412 and NACA 23012 was higher than the other profiles. [5] In this paper, a stable and aerodynamic design using NACA 4412 profile with blade length (800 mm) and power (600 W) with mini HAWT was pro-posed. The length chord and twist angle distributions of the initial blade model were calculated. A reasonable compromise between high efficiency and good starting torque was obtained. The blades were developed using MATLAB software. The op-timized blade chord was reduced by 24% and the thickness by 44%. The power level of the optimized blade was significantly increased to 30% compared to the standard blade. [6] This paper explained the design and optimization of a small HAWT blade using custom code. The blades were made using NACA 4412, NACA 2412 and NACA 1812 at a wind speed of 5 m/s, which was the most frequent wind speed pre-ailing in the Indian peninsula. Based on a self-created code based on BEM theory, an optimum blade profile was generated which performs with high efficiency using multiple airfoils. The twist angle distribution, chord distribution and other parame-ters for different airfoil sections along the blade were determined using the proposed code. For a rotor with a diameter of 4.46 m, a power factor of 0.490 and an output power of 0.56 kW was obtained. The blade analysis result obtained using Q-blade software showed reliable agreement with the proposed code and wind turbine per-formance analysis. The power factor obtained using the MATLAB code was 0.490, which was very close to that obtained using Q-blade (0.514). In addition, the differ-ence in output power between the two values was only 28.58 W. [7] The behaviour and performance of a multi-section HAWT blade with and without a fence are researched in this paper. The multi-section HAWT blade was designed using supercritical airfoils (SG6043, FX63-137S and FX66-S-196V). The overall performance of the multi-section blade was compared with the single-section NACA4412 blade. Numerical analyses were performed using the author's code (Fortran 90) and the Qblade package based on BEM theory. The multi-pass vanes show an increase of about 8% in power factor compared to the single-pass vanes. The boundary layer theory was used to design the fences and their

position was de-termined experimentally. An increase in total power factor of about 16% with the use of fences and high flutter stability.

[8] This paper investigated the aero-elastic behavior of horizontal axis wind turbine (HAWT) flexible blades by using computational and aerodynamic models approach. To study the unstable blade airfoil aerodynamic properties, the B-L (Beddoes-Leishman) dynamic stall model was added to the modified Blade Element Momentum (BEM) model. [9] In this paper investigation of the aero-elastic model of multi-rotor HAWT was done. The method used in this system was to integrate the single-rotor HAWCStab2 with the multi-rotor tool HAWC2. Therefore, this method of fidelity linear time-invariant aero elastic modelling was verified by comparing the frequency responses of different rotors. [10] This paper studied the aero elastic behavior of a MW (multi-megawatt) HAWT is influenced by the integrity of the aero-dynamic simulation. The main purpose of this research is the comparison between engineering model results and CFD aero elastic simulations results that needs less empirical modeling. To investigate the influence of the aerodynamic models on the aero elastic results for large HAWT, two distinct models (BEM- and CFD-based) were used. [11] The two-part study looks at horizontal axis wind turbines which have improved aero elastic performance and hence boost yearly energy output is proposed in this paper. The structural characteristics of a standard blade were then idealized using an adaptable shear. This development's power curve is evaluated, and it is proven to dramatically boost yearly energy output over traditional systems by 1.51 % than the maximum power at a wind speed of 15 m/s. [12] Researchers developed the URANS equations that were integrated with the FEM in a flexible way to describe the aero-elastic behaviour of Tjreborg horizontal axis wind turbine blades. At four different horizontal inflow wind speeds, this approach was validated by comparing simulated and experimental data. The aero-elastic behaviour of the Tjreborg wind turbine was also estimated and studied for yaw angles of 10, 30, and 60 degrees. [13] This research was done by developing a horizontal axis wind turbine rotor blade model for showing the coupling effect of rotor bulk rotation and blade flexible motion. The model was created with Lagrange's technique, as well as the blade was discretized utilizing the finite element method (FEM). The two different relationships between aerodynamics wind and structural behavior are captured in this design. [14] Researchers developed a wind speed model for n-blades of horizontal axis wind turbines with the considerations of wind shear and buildings shadow impacts. The systematic approach was utilized to calculate the wind shear, building shadows, synthesis, and equivalent wind velocity disturbances elements, as well as their relative positions in the rotor disc region. [15] This paper investigated the influence of diagonally input upon the wake parameters of a HAWT (Horizontal Axis Wind Turbine) inside a wind farm. A HAWT with a generator limit of 30 kW and then rotor diameter of 10.0 m was employed in this work. A field study was used to analyse the influence of tilt angle on the energy and thrust efficiency of a HAWT. On this foundation, the HAWT's wake properties were investigated with various wind orientations and pitch angles. As a result, the peak power coefficients C_p were 0.31, 0.33, and 0.27, respectively, and correlate to tip velocity ratios $\lambda = 7.5, 7.4,$ and 6.8 with pitch angles $\beta = 0^\circ, 2^\circ,$ and 4° . The wind turbine experimental model predicts around 51% of annual power generation compared to the experimental research model.

In this study, the behavior and performance of different blade cross-sections, symmetrical, asymmetrical and supercritical airfoils (NACA0012, NACA 4412 and EPPLER 417) were investigated experimentally and by ANSYS. The horizontal axis wind turbine blade design was performed using Fortran 90 code and QBlade software based on BEM theory.

2. THE BLADE CROSS-SECTION

Table 1 shows the airfoil characteristics in cross sections and the airfoil shapes are shown in Figure 1. The HAWT rotor design parameters are shown in Table 2.

Table 1 Cross-Section Airfoils Distribution

| Airfoil | Max t/c | Max Cl/Cd |
|------------|-----------------|----------------|
| NACA 4412 | 12% at 30% | 129.4 at 5.25° |
| NACA 0012 | 12% at 30% | 75.6 at 7.5° |
| EPPLER 417 | 14.2% at 38.35% | 135.9 at 2.25° |

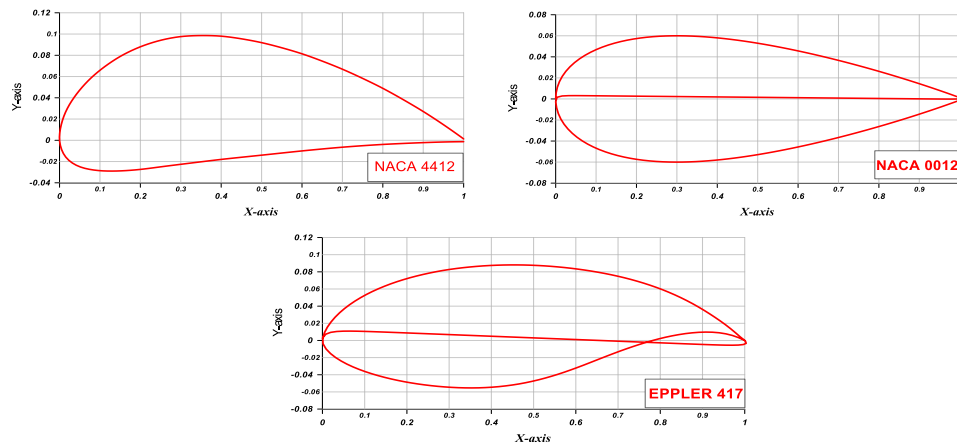


Fig. 1 Airfoils geometry

Table 2 Parameter of Design

| | |
|------------------|--------------------|
| Rotor Diameter | 1.07 m |
| Hub Diameter | 0.20 m |
| Number of Blades | 3 |
| Rated Power | 600 W |
| Cut in Speed | 2 m/s ² |

3. POWER COEFFICIENT

Fig. 2 shows maximum power that can be produced by wind flowing through the ring. [7]. The velocity around the disc is assumed to be constant ($U_2 = U_3$) with the assumption that the upstream and downstream pressures are equal. The equations yield the rotor power coefficient. Equations [16].

$$U_2 = \frac{U_1 + U_4}{2} \quad (1)$$

$$a = \frac{U_1 - U_2}{U_1} \quad (2)$$

$$U_2 = U_1 (1 - a) \quad (3)$$

$$U_4 = U_1 (1 - 2a) \quad (4)$$

$$P = \int_{r_h}^R dP = \int_{r_h}^R \Omega dQ \quad (5)$$

$$C_p = \frac{P}{P_{wind}} = \frac{\int_{r_h}^R \Omega dQ}{\frac{1}{2} \rho R^2 U_1^3} \quad (6)$$

$$C_p = \left(\frac{8}{\lambda^2} \right) \int_{\lambda_h}^{\lambda} \lambda_r^3 a(1-a) \left[1 - \left(\frac{C_d}{C_l} \right) \cot \varphi \right] d\lambda_r \quad (7)$$

The tip speed ratio;

$$\lambda = \frac{2R\pi N}{60U_1} \quad (8)$$

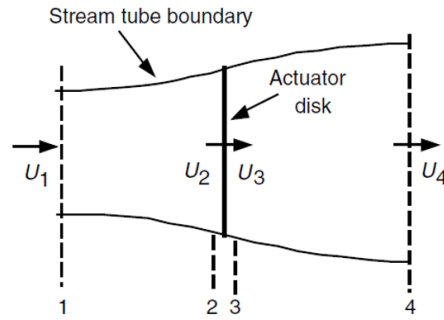


Fig. 2 Wind turbine actuator disk model

4. DESIGN AND MANUFACTURING BLADES

A program in FORTRAN (f.90) was written and the Qblade package was used to calculate the aerodynamic data and power factor based on Blade Element Momentum (BEM) theory, as shown in Tables 3, 4 and 5 and Figure 3. Solidworks software was used to design the 3D blade shapes (see Figure 4). The developed models were fabricated on a 3D printer (see Figure 5). Due to the limited size of the printer's print area, the blades were divided into several sections and then combined. The blades with different profiles in sections (NACA 4412, NACA 0012 and EPPLER 417) were mounted to the wind turbine for testing as shown in Figure 6.

Table 3 NACA 4412 Cross-Section Geometry

| | Position (m) | Chord (m) | Twist (deg) | Foil |
|----|--------------|-----------|-------------|-----------|
| 1 | 0.00 | 0.167 | 43.42 | NACA 4412 |
| 2 | 0.10 | 0.156 | 23.14 | NACA 4412 |
| 3 | 0.17 | 0.136 | 16.72 | NACA 4412 |
| 4 | 0.27 | 0.109 | 10.91 | NACA 4412 |
| 5 | 0.37 | 0.090 | 7.42 | NACA 4412 |
| 6 | 0.47 | 0.076 | 5.11 | NACA 4412 |
| 7 | 0.57 | 0.066 | 3.47 | NACA 4412 |
| 8 | 0.67 | 0.058 | 2.25 | NACA 4412 |
| 9 | 0.77 | 0.052 | 1.30 | NACA 4412 |
| 10 | 0.87 | 0.046 | 0.56 | NACA 4412 |
| 11 | 0.97 | 0.042 | -0.05 | NACA 4412 |
| 12 | 1.07 | 0.038 | -0.56 | NACA 4412 |

Table 4 NACA 0012 Cross-Section Geometry

| | Position (m) | Chord (m) | Twist (deg) | Foil |
|----|--------------|-----------|-------------|-----------|
| 1 | 0.00 | 0.206 | 41.43 | NACA 0012 |
| 2 | 0.10 | 0.194 | 21.14 | NACA 0012 |
| 3 | 0.17 | 0.168 | 14.72 | NACA 0012 |
| 4 | 0.27 | 0.136 | 8.91 | NACA 0012 |
| 5 | 0.37 | 0.112 | 5.42 | NACA 0012 |
| 6 | 0.47 | 0.094 | 3.11 | NACA 0012 |
| 7 | 0.57 | 0.082 | 1.47 | NACA 0012 |
| 8 | 0.67 | 0.072 | 0.25 | NACA 0012 |
| 9 | 0.77 | 0.064 | -0.69 | NACA 0012 |
| 10 | 0.87 | 0.057 | -1.44 | NACA 0012 |
| 11 | 0.97 | 0.052 | -2.05 | NACA 0012 |
| 12 | 1.07 | 0.048 | -2.56 | NACA 0012 |

Table 5 EPPLER 417 Cross-Section Geometry

| | Position (m) | Chord (m) | Twist (deg) | Foil |
|----|--------------|-----------|-------------|------------|
| 1 | 0.00 | 0.283 | 47.42 | EPPLER 417 |
| 2 | 0.10 | 0.266 | 27.14 | EPPLER 417 |
| 3 | 0.17 | 0.231 | 20.72 | EPPLER 417 |
| 4 | 0.27 | 0.186 | 14.90 | EPPLER 417 |
| 5 | 0.37 | 0.153 | 11.42 | EPPLER 417 |
| 6 | 0.47 | 0.129 | 9.11 | EPPLER 417 |
| 7 | 0.57 | 0.112 | 7.47 | EPPLER 417 |
| 8 | 0.67 | 0.098 | 6.25 | EPPLER 417 |
| 9 | 0.77 | 0.087 | 5.31 | EPPLER 417 |
| 10 | 0.87 | 0.079 | 4.55 | EPPLER 417 |
| 11 | 0.97 | 0.072 | 3.94 | EPPLER 417 |
| 12 | 1.07 | 0.066 | 3.44 | EPPLER 417 |

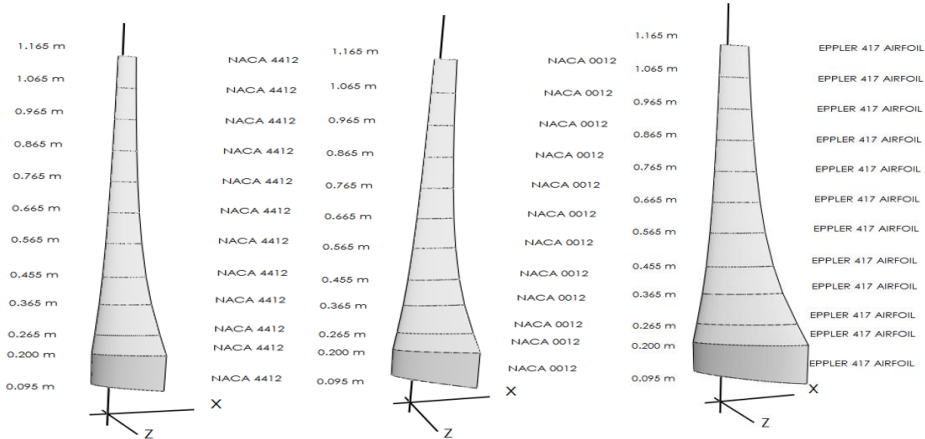


Fig. 3 Cross-section blades by Qblade package

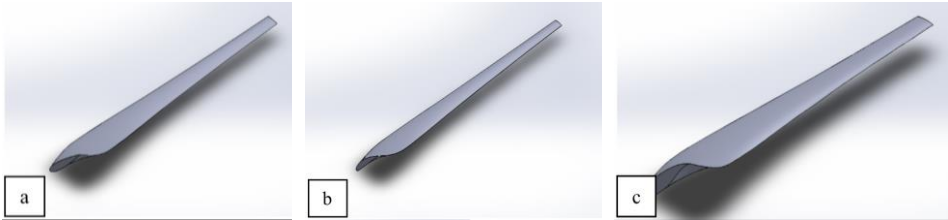


Fig. 4 Cross-section blade by SolidWorks (a) NACA 4412 Blade (b) NACA 0012 Blade (c) EPPLER 317 Blade



Fig. 5 3D Printing Process



Fig. 6 Wind turbines (a) with NACA4412 cross-section blades (b) with NACA0012 cross-section blades (c) with EPPLER 317 cross-section blades

The material assigned to the blades was carbon fiber and its properties are shown in Figure 7. Applied pressure was 14.25 MPa, 251 MPa, 986.4 MPa and 1370 MPa to derive the post-processing results of Total Deformation, Equivalent Stress and Equivalent Strain shown in Table 7.

| Properties of Outline Row 3: Carbon Fiber (230 GPa) | | | |
|---|-----------------------------|------------|--------------------|
| | A | B | C |
| 1 | Property | Value | Unit |
| 2 | Density | 1800 | kg m ⁻³ |
| 3 | Orthotropic Elasticity | | |
| 4 | Young's Modulus X direction | 2.3E+11 | Pa |
| 5 | Young's Modulus Y direction | 2.3E+10 | Pa |
| 6 | Young's Modulus Z direction | 2.3E+10 | Pa |
| 7 | Poisson's Ratio XY | 0.2 | |
| 8 | Poisson's Ratio YZ | 0.4 | |
| 9 | Poisson's Ratio XZ | 0.2 | |
| 10 | Shear Modulus XY | 9E+09 | Pa |
| 11 | Shear Modulus YZ | 8.2143E+09 | Pa |
| 12 | Shear Modulus XZ | 9E+09 | Pa |
| 13 | Tensile Yield Strength | 2500 | MPa |

Fig. 7 Carbon Fiber Properties

5. RESULTS AND DECISIONS

The primary design element of a wind turbine blade is the cross-sectional area of the airfoil, which transforms the airflow velocity into a pressure distribution throughout the length of the blade. In this investigation, many profiles including symmetrical, asymmetrical, and supercritical have been used. When evaluating the performance of the profiles, the primary factors to consider are the amount of energy absorbed from the free stream, the maximum lift-to-drag ratio, and the angle of attack. Not just the power factor peak, but also the airfoil's overall cross-sectional efficiency, was taken into account.

Figure 8 demonstrates that compared to the other profiles, the EPPLER 417 profile produced less drag. Additionally, as shown in Figure 9, the Eppler 417 profile produced the greatest pressure dispersion in the second third of the blade radius. As indicated in Fig. 10, the NACA 4412 profile had the highest power factor value ($C_p = 0.516$), followed by the NACA 0012 ($C_p = 1.491$), and the Eppler 417 ($C_p = 0.510$) profiles. However, according to Figure 11, the Eppler 417 profile had the highest overall efficiency.

According to the experimental findings (see Table 6), Eppler 417 performs the best and produces the most power of the other profiles. CFD results showed that NACA 4412 goes through less deformation and stresses (Figures 12 to 17 and Table 7).

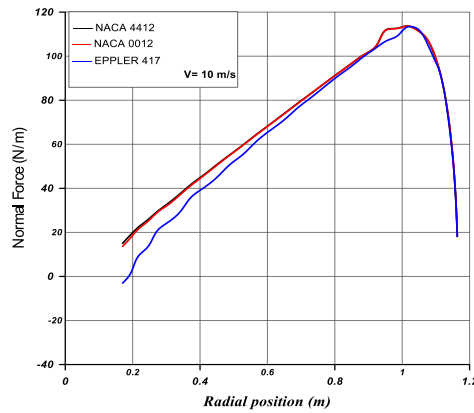


Fig. 8 Normal force distribution along the blades radius

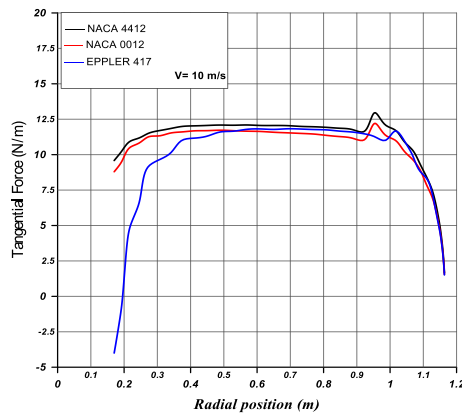


Fig. 9 Tangential force distribution along the blades radius

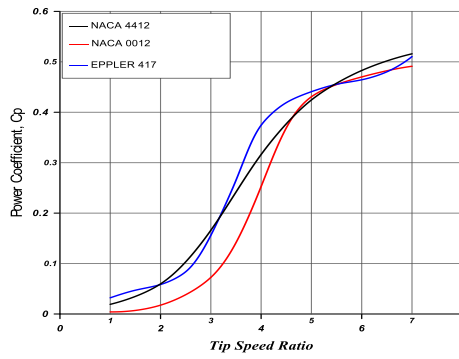


Fig. 10 The power coefficient of the cross-sections blades versus tip speed ratio

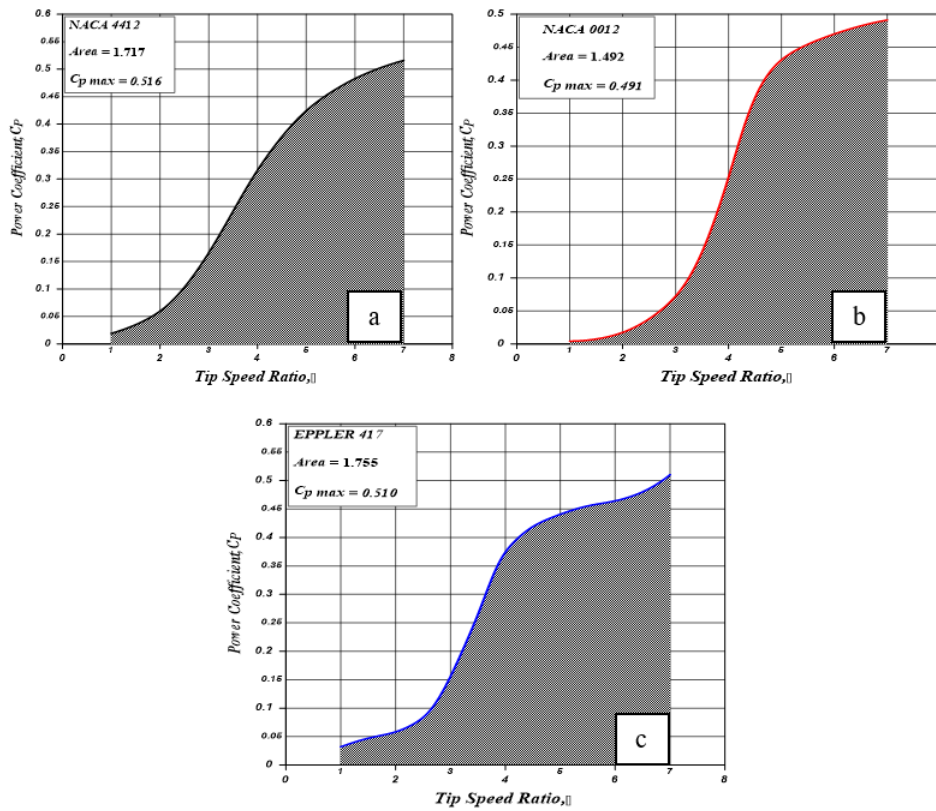


Fig. 11 The area under power coefficient curve (a) NACA 4412 cross-section blade (b) NACA 0012 cross-section blade (c) EPPLER 317 cross-section blade

Table 6 Experimental Results

| Wind speed (m/s) | NACA 4412 | | NACA 0012 | | EPPLER 417 | |
|------------------|-----------|---------|-----------|---------|------------|---------|
| | rpm | Power W | rpm | Power W | rpm | Power W |
| 3 | 62 | 13 | 51 | 10 | 68 | 20 |
| 4.2 | 88 | 93 | 69 | 28 | 95 | 122 |
| 5.4 | 107 | 144 | 96 | 125 | 122 | 173 |
| 6.5 | 125 | 306 | 114 | 285 | 147 | 330 |
| 7.5 | 171 | 506 | 132 | 363 | 178 | 546 |

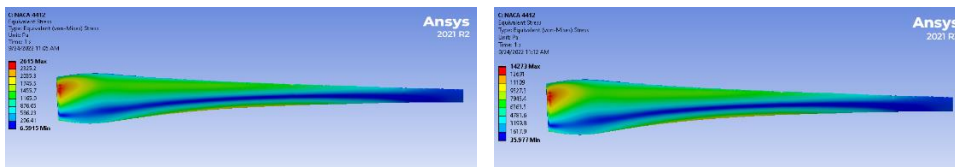


Fig. 12 Equivalent Stress for NACA 4412 at 251 Pa and 1370 Pa

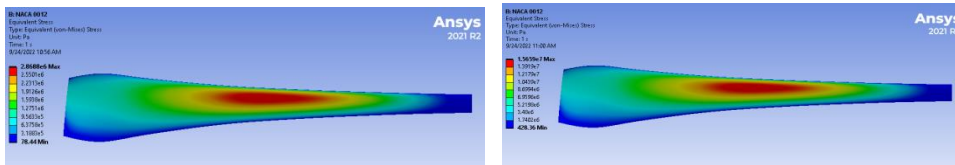


Fig. 13 Equivalent Stress for NACA 0012 at 251 Pa and 1370 Pa

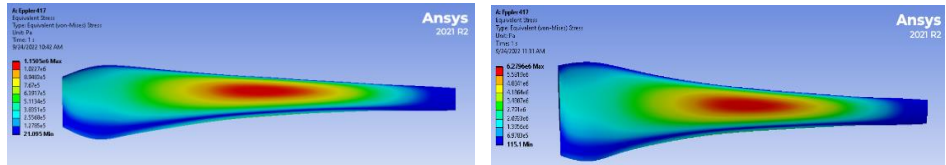


Fig. 14 Equivalent Stress for EPPLER 417 at 251 Pa and 1370 Pa

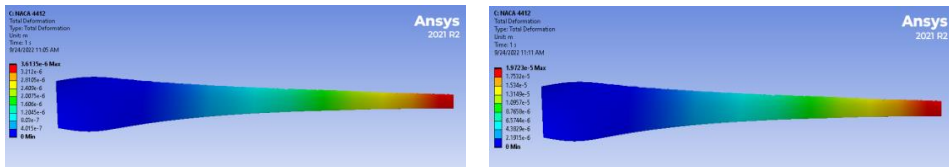


Fig. 15 Total Deformation for NACA 4412 at 251 Pa and 1370 Pa

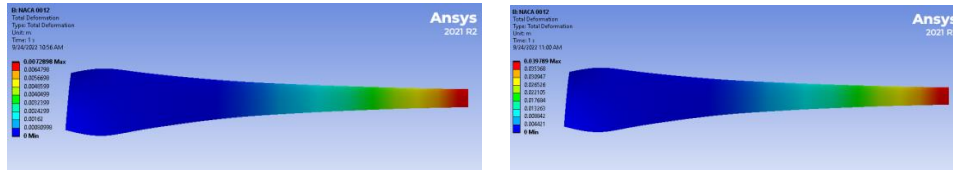


Fig. 16 Total Deformation for NACA 0012 at 251 Pa and 1370 Pa

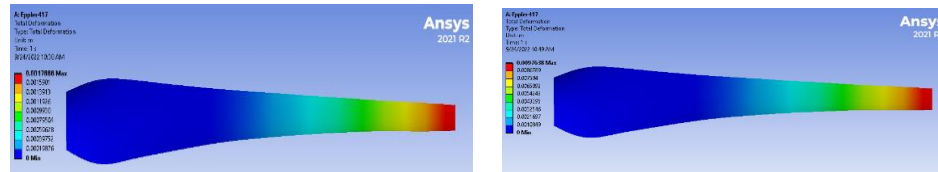


Fig. 17 Total Deformation for EPPLER 417 at 251 Pa and 1370 Pa

Table 7 CFD Results

| Blade Models | Applied Pressure (Pa) | Total Deformation (mm) | Equivalent Stresses (MPa) | Equivalent Strain (mm/mm) |
|--------------|-----------------------|------------------------|---------------------------|---------------------------|
| EPPLER 417 | 14.25 | 0.1016 | 0.0653 | 3.49E-06 |
| | 251 | 1.7888 | 1.1505 | 6.15E-05 |
| | 986.4 | 7.0299 | 4.5213 | 2.42E-04 |
| NACA 0012 | 14.25 | 0.4138 | 0.1628 | 8.70E-06 |
| | 251 | 7.2898 | 2.8688 | 1.53E-04 |
| | 986.4 | 28.648 | 11.274 | 6.02E-04 |
| NACA 4414 | 14.25 | 2.05E-04 | 1.49E-04 | 8.13E-09 |
| | 251 | 3.61E-03 | 2.62E-03 | 1.43E-07 |
| | 986.4 | 1.42E-02 | 0.01028 | 5.63E-07 |
| | 1370 | 1.97E-02 | 0.01427 | 7.81E-07 |

6. CONCLUSIONS

The effects of several cross-section airfoil types on the effectiveness of HAWT blade efficiency were studied. Analysis was done on three different airfoils: supercritical (EPPLER 417), asymmetric (NACA 0012), and symmetric (NACA 4412). The analyses that were performed combined theory and experiment. Theoretical analyses were carried out using Fortran 90 code and the blade element momentum-based Qblade code. The findings of experimental tests supported the conclusions of the theory. At a short angle of attack, supercritical airfoils always produce the highest lift-to-drag ratio. EPPLER 417 has a high chord length and twist angle, so it generates the highest power.

Since the CFD results show that NACA 4412 has less total deformation and equivalent stress. This is due to the reason that NACA 4412 has a greater cross-section area and stress is inversely proportional to the area.

Overall EPPLER 417 is the optimum blade cross-section as it produces more power and has less deformation than the NACA 0012.

REFERENCES

- [1] B. Somaiday, I. Czajkal, M. A. R. Yass, "The Influence of Cross-Section Airfoil on The HAWT Efficiency", In Proceedings of the 7th Virtual International Conference on Science, Technology and Management in Energy (eNergetics 2021), Belgrade, Serbia, 16-17 2021, pp. 545-551.
- [2] C. Bak et al., "Wind tunnel test on wind turbine airfoil with adaptive trailing edge geometry", In Proceedings of the 45th AIAA Aerospace Sciences Meeting and Exhibit, 2007, p. 1016.
- [3] D. G. Hull, *Fundamentals of airplane flight mechanics*, vol. 19. Springer, 2007.
- [4] N. Tenguria, N. D. Mittal and S. Ahmed, "Evaluation of performance of horizontal axis wind turbine blades based on optimal rotor theory", *J. Urban Environ. Eng.*, vol. 5, no. 1, pp. 15-23, 2011.
- [5] S. A. Kale and R. N. Varma, "Aerodynamic design of a horizontal axis micro wind turbine blade using NACA 4412 profile", *Int. J. Renew. Energy Res.*, vol. 4, no. 1, pp. 69-72, 2014.
- [6] F. Javed, S. Javed, T. Bilal and V. Rastogi, "Design of multiple airfoil HAWT blade using MATLAB programming", In Proceedings of the IEEE International Conference Renewable Energy Resources Application, 2016, pp. 425-430.
- [7] A. H. Muheisen, M. A. R. Yass and I. K. Irthiea, "Enhancement of Horizontal Wind Turbine Blade Performance Using Multiple Airfoils Sections and Fences", *J. King Saud Univ. - Eng. Sci.*, 2021.
- [8] W. W. Mo, D. Y. Li, X. N. Wang, C. T. Zhong, "Aeroelastic coupling analysis of the flexible blade of a wind turbine", *Energy*, vol. 89, pp. 1001-1009, 2015.
- [9] O. T. Filsoof, A. Yde, P. Böttcher and X. Zhang, "On Critical Aeroelastic Modes of a Tri-rotor Wind Turbine", *Int. J. Mech. Sci.*, p. 106525, 2021.
- [10] M. Sayed, L. Klein, Th. Lutz and E. Kramer "The impact of the aerodynamic model fidelity on the aeroelastic response of a multi-megawatt wind turbine", *Renew Energy*, vol. 140, pp. 304-318, 2019.
- [11] M. Capuzzi, A. Pirrera and P. M. Weaver, "A novel adaptive blade concept for large-scale wind turbines. Part II: Structural design and power performance", *Energy*, vol. 73, pp. 25-32, 2014.
- [12] L. Dai, Q. Zhou, Y. Zhang, S. Yao, S. Kang and X. Wang, "Analysis of wind turbine blades aeroelastic performance under yaw conditions", *J. Wind Eng. Ind. Aerod.*, vol. 171, pp. 273-287, 2017.
- [13] D. Ju and Q. Sun, "Modeling of a wind turbine rotor blade system", *J. Vib. Acoust. Trans. ASME*, vol. 139, pp. 1-15, 2017.
- [14] S. Wan, L. Cheng and X. Sheng, "Numerical analysis of the spatial distribution of equivalent wind speeds in large-scale wind turbines", *J. Mech. Sci. Technol.*, vol 31, no. 2, pp. 965-974, 2017.
- [15] Y. Wang, Y. Kamada, T. Maeda, J. Xu, S. Zhou, F. Zhang and C. Cai, "Diagonal inflow effect on the wake characteristics of a horizontal axis wind turbine with Gaussian model and field measurements", *Energy*, vol 238, p. 121692, 2022.
- [16] M. Ragheb and A. M. Ragheb, "Wind turbines theory-the betz equation and optimal rotor tip speed ratio", *Fundam. Adv. Top. Wind power*, vol. 1, no. 1, pp. 19-38, 2011.
- [17] M. A. R. Yass, "Highest Power Coefficient of Horizontal Axis Wing Turbine (HAWT) Using Multiple Airfoil Section", *Test Eng. Manag.*, vol. 83, pp. 30029-30041, 2020.